Determination of atmospheric column condensate using active and passive remote sensing technology

Huige Di [1], Yun Yuan [1], Qing Yan [1], Wenhui Xin [1], Shichun Li [1], Jun Wang [1], Yufeng Wang [1], Lei Zhang [2], Dengxin Hua [1]*

[1]School of Mechanical and Precision Instrument Engineering, Xi'an University of Technology, Xi'an 710048, China
[2]College of Atmospheric Sciences, Lanzhou University, Lanzhou 730000, China

Correspondence to: Dengxin Hua (dengxinhua@xaut.edu.cn)

Abstract. To further exploit atmospheric cloud-water resources (CWRs), it is necessary to correctly evaluate the amount of CWRs in an area. CWRs are hydrometeors that have not participated in precipitation formation at the surface and are suspended in the atmosphere to be exploited and maximize possible precipitation in the atmosphere (Zhou, Y., et al. (2020)). CWRs include three items: the existing hydrometeors at a certain time, the influx of atmospheric hydrometeors along the boundaries of the study area, and the mass of hydrometeors converted from water vapor through condensation or desublimation, defined as condensate. Condensate constitutes the most important part of CWRs. At present, there is a lack of effective observation methods for atmospheric column condensate evaluation, and direct observation data of CWRs are thus insufficient. A detection method for atmospheric column condensate is proposed and presented. The formation of condensate is closely related to atmospheric meteorological parameters (e.g., temperature and vertical airflow velocity). The amount of atmospheric column condensate can be calculated by the saturated water vapor density and the ascending velocity at the cloud base and top. Active and passive remote sensing technologies are applied to detect the mass of atmospheric column condensate. Combining millimeter-wave radar, lidar and microwave radiometers can suitably observe the vertical velocity and temperature at the cloud boundary. The saturated vapor density can be derived by the temperature, and then, water vapor flux and the maximum possible condensate can be deduced. A detailed detection scheme and data calculation method are presented, and the presented method can realize the determination of atmospheric column condensate. A case of cloud layer change before precipitation is considered, and atmospheric column condensate is deduced and obtained. This is the first application, to our knowledge, of observations for atmospheric column condensate evaluation, which is significant for research on the hydrologic cycle and the assessment of cloud water resources.

1 Introduction

Water is a renewable but finite natural resource. Although three-quarters of the Earth's surface is covered with water, the freshwater resources available for human uses are very limited. The availability varies significantly over space and time. With the increasing in water consumption caused by the human population, freshwater will become an increasingly scarce

30   resource in the future (Yoshiaki et al., 2009). In principle, freshwater resources all originate from precipitation. Precipitation, produced by the atmospheric water cycle, is the main source of river runoff and shallow underground freshwater that can be directly used by humans (Zhou et al., 2020). The atmospheric water cycle is one of the branches of the water cycle (Su et al., 2014). The former process arises from evaporation of oceans, lakes and rivers, and water vapor is then transported within the atmosphere and condenses into clouds; finally, water is precipitated onto the ground before evaporating again (Yao et al.,

35   2020). Atmospheric water includes water vapor and hydrometeors (also referred to as cloud water in both liquid and solid phases). The atmospheric water vapor resources on Earth are very abundant, while water vapor cannot directly be precipitated, and only the water substance that has experienced the secondary phase change and has turned into the liquid/solid phase may form rainfall, which is defined as CWRs (Zhou et al., 2020). CWRs refers to hydrometeors that participate in atmospheric water change in a certain area and time period but have not formed ground precipitation and thus

40   can be utilized/exploited (Jalihal et al., 2019). The formation of hydrometers is affected by dynamic and thermodynamic processes in the atmosphere, which play an important role in the global water cycle.

    Arid and semiarid areas cover more than half of China's land area. Water shortages are serious in China. It is an urgent task to rationally develop CWRs in the atmosphere. Approximately 14%~18% of water vapor in air can condense into cloud water and be precipitated onto the ground, so there is still a great potential for the development of CWRs. It is of great

45   strategic significance to carry out comprehensive research of the development and application of atmospheric water resources and realize the optimal allocation of CWRs to alleviate the current situation of uneven drought and flooding in China. The first step of exploiting CWRs is to correctly evaluate CWRs in an area, that namely, the potential precipitation of the cloud system. At present, the evaluation of CWRs is mainly based on reanalysis data or mesoscale numerical simulations (Zhou et al., 2011). Due to a lack of observation data of CWRs, the evaluation results of CWRs using numerical simulations

50   have not been verified, which greatly affects the effectiveness and economic applicability of weather modification. It is urgent to develop instruments and methods that can observe CWRs.

    The CWRs are closely related to various macro- and microparameters of clouds and multiple atmospheric parameters, and these resources mainly depend on the distribution of the water vapor supply and updraft (Jalihal et al., 2019). Researchers have carried out many observations of the macro- and microphysical characteristics of clouds through ground-based, aircraft

55   and satellite equipment (Williams et al., 2016; Chetankumar Jalihal, et al. 2019; Liu et al., 2013; Si et al., 2019). Meteorological satellites can provide a more accurate assessment of the global cloud distribution. The cloud products provided by meteorological satellites mainly include cloud cover, cloud water paths, cloud optical thickness, and other factors. In previous studies, the cloud water path was generally regarded in CWRs evaluation. According to the definition of CWRs proposed by Zhou et al. (Zhou et al., 2020), the state quantity of hydrometeors represents only a small part of the

60   CWRs (Zhou et al., 2011). The mass of hydrometeors converted from water vapor due to updraft through condensation or desublimation is an important part. However, there are no methods or means for the observation of cloud water caused by updraft.

Supported by the National Natural Science Foundation of China's Major Research Instrument Development project, Xi'an University of Technology and Lanzhou University carried out a study of cloud potential precipitation assessment and observation technology, focusing on remote sensing detection and atmospheric column condensation. Based on the formation mechanism of condensate in the atmosphere, this paper proposes a method of atmospheric column condensate detection. Remote sensing technologies combining lidar, millimeter wave radar and microwave radiometry were used for the determination of atmospheric column condensate, and experimental observations were carried out.

2 CWRs

According to the atmospheric water cycle process, only water condensate in clouds can grow into raindrops to form precipitation, and the potential precipitation refers to the total mass of cloud water in a certain region and period, including the amount of cloud water in the region at the beginning of a given period, the amount of cloud water input horizontally during the period and the amount of condensed cloud water vertically. Fig. 1 shows a schematic diagram of CWRs. The horizontal arrows represent the cloud water horizontally oriented input or output from the cloud side boundary, the vertical arrow represents the cloud water coming in and out of the cloud top or cloud bottom through updraft or downdraft, and blue dots indicate the cloud water already in the cloud.
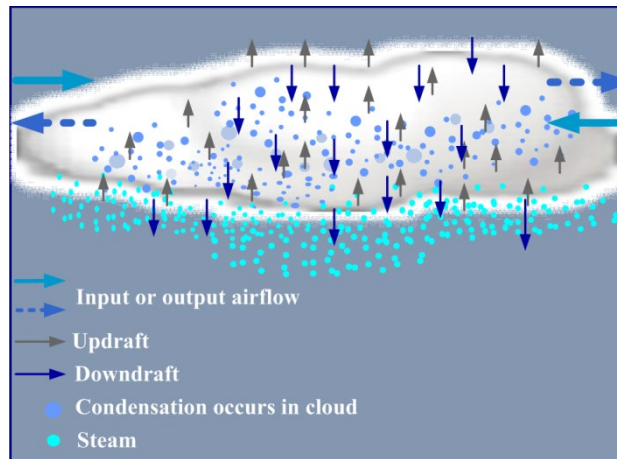
Figure 1: Schematic diagram of CWRs

Based on the atmospheric water substance budget and water mass conservation, for an atmospheric column extending from the ground to the top of the atmosphere, the budget equation of atmospheric hydrometeors can be expressed follows (Zhou et al., 2020).

$$M_{h1} + Q_{hi} + C_{vh} = M_{h2} + Q_{ho} + C_{hv} + P_S = GM_h , \tag{1}$$

The left side of the equation is the income item of the atmospheric hydrometeors, and the middle is the expenditure item. M_{h1} and M_{h2} are the masses of hydrometeors at time t_1 and t_2, respectively. Q_{hi} and Q_{ho} are the influx and outflux, respectively, of atmospheric hydrometeors along the boundaries of the study area. C_{vh} is the mass of hydrometeors converted from water

vapor through condensation or sublimation, and C_{hv} is the mass content of water vapor converted from hydrometeors through evaporation or sublimation. P_S is the surface precipitation. GM_h is the gross mass of atmospheric hydrometeors, representing the total amount of hydrometeors during period $t_2 - t_1$ within the study region.

M_{h1} at time t_1, namely, the cloud liquid water content (CLW) and ice water content (IWC), can be observed with remote sensing instruments, such as cloud radar, microwave radiometer and imaging spectroradiometer instruments (Hengchi et al., 2003). Many spaceborne observations of the column-integrated cloud liquid water path (LWP) exist. After many years of development, the inversion algorithm of the CLW using satellite remote sensing data is now mature (Jussi et al. 2016). Q_{hi} and Q_{ho} are related to the horizontal wind speed and cloud water content, respectively, along the boundary, which can be measured by wind profiler and cloud radars, respectively. In addition to the existing cloud water and horizontal inputs, the mass content of water vapor converted from hydrometeors through evaporation or sublimation accounts for a large proportion of cloud water resources. Updraft and sufficient water vapor are necessary for cloud formation. To a certain extent, the condensate produced by updraft is the main indicator of whether the cloud system can produce rainfall. Regarding synoptic-scale and mesoscale precipitation processes, the mass of condensate is 100 and 10 times larger, respectively, than the cloud water input from the side boundary.

3 Atmospheric column condensate

The cloud system is a saturated wet system with containing liquid water (or ice particles), which is a binary multiphase system. When water vapor below clouds is transported to the upper space (cloud layer) by updraft and the transported water vapor reaches saturation in cooler air, the excess water vapor will condense and form water condensate (Gu et al., 2006). The condensate produced by updraft in cloud systems cannot be directly observed and quantified similarly to the above CLW. Most of the important thermal processes in the atmosphere, especially the vertical motion of air, can be considered adiabatic processes. Therefore, atmospheric column condensate can be estimated by the saturated water vapor density and the ascending velocity at the cloud base. Of course, not all the water vapor entering the cloud layer from the base can be transformed into condensate. A part of the water vapor will escape if updraft occurs at the cloud top. It is also possible that some water vapor does not condense and exists in the cloud as supersaturated water vapor. However, it is certain that the more water vapor enters the cloud, the more condensate may be generated. If we can obtain the saturated water vapor density and vertical air velocity at the cloud base and top, we can obtain the instantaneous water vapor flux into the cloud. If the temperature at the cloud top is lower than that at the cloud base, it can be considered that most of the water vapor entering the cloud has condensed. It is assumed that the water vapor condensation efficiency is k, and its value is less than 1. We focus on the maximum possible condensate content, so k is set to 1 in this paper. The total hydrometer flux of the atmosphere per unit area during this period can be obtained by integrating the flux over this period, and the atmospheric column condensate can be expressed with Equations (2) to (5):

$$P_{wv} = P_{wv\_in} - P_{wv\_out},$$

(2)

$$P_{wv\_in} = \int_{t_1}^{t_2} S_{base}(T) v_{base}(t) dt \, , \tag{3}$$

$$P_{wv\_out} = \int_{t_1}^{t_2} S_{top}(T) v_{top}(t) dt \, , \tag{4}$$

120
$$\begin{aligned} P_{cong} &= k \cdot \left(P_{wv\_in} - P_{wv\_out} \right) \\ &= k \cdot \int_{t_1}^{t_2} \left(S_{base}(T) \cdot v_{base}(t) - S_{top}(T) \cdot v_{top}(t) \right) dt \, , \end{aligned} \tag{5}$$

where p_{wv_in} is the input water vapor flux from the cloud base, p_{wv_out} is the output water vapor flux from the cloud top, and p_{wv} is the water vapor flux remaining in the cloud layer during the period from t_1 to t_2. S is the saturated water vapor density, which is related to the atmospheric temperature and the unit is g/m^3, and the subscripts base and top refer to the cloud base and cloud top, respectively, v is the vertical velocity of the airflow, and the unit is m/s, a downward value is negative and an

125 upward value is positive. p_{cong} is the flux of hydrometeors converted from water vapor through condensation or sublimation during the period from t_1 to t_2.

Based on the ideal gas equation of state, the relationship between the water vapor density ρ_v and atmospheric temperature T is in accordance with the following equation:

$$\rho_v = \frac{e}{R_v T} = \frac{\varepsilon e}{R_d T} \, , \tag{6}$$

130 where ε is 0.622, R_d is a constant for dry air (287.05 J/kg·K), T is the absolute temperature (K), and e is the water vapor pressure (hPa). The saturated water vapor density can be derived from the saturated water vapor pressure at the same temperature. From the Tetens empirical equation, the saturated vapor pressure $e_S(T)$ of the liquid surface at temperature T can be written as

$$e_s(T) = 610.78 \times \exp[17.2693882(T - 273.16)/(T - 35.86)] \, , \tag{7}$$

135 If the temperature is below 0 °C, the value of $e_S(T)$ should reach

$$e_s(T) = 611.2 \times \exp[17.67(T - 273.15)/(T - 29.65)] \, . \tag{8}$$

The atmospheric column condensate can be determined by the vertical velocity of airflow and the temperature difference between the cloud base and cloud top. If the detected cloud layer is very thick (> 3 km), the temperature at the cloud top will be much lower than that at the base, and the saturated water vapor density at the cloud top will be a very small value, so the

140 water vapor term overflowing from the cloud top can be ignored. If the cloud layer is thin, such as a stratiform cloud, the water vapor from the cloud top cannot be ignored. Otherwise, this could cause serious errors in the condensate calculation.

4. Feasibility analysis of remote sensing observations for atmospheric column evaluation

If the temperature and vertical air velocity at the cloud base and cloud top can be obtained over a certain period, the condensate generated in the cloud layer during this period can be derived according to Eq. (6). It is difficult to continuously observe vertical flow at the cloud base and cloud top. Observation instruments with high temporal and spatial resolutions are needed. Remote sensing instruments can realize continuous observation of atmospheric parameters. During the period of cloud change, the vertical air velocity near and within the cloud deck varies rapidly and greatly. The vertical air velocity of stratiform clouds is very low, usually lower than 1 m/s. The vertical air velocity at the base of cumulonimbus clouds is relatively high and develops rapidly. The large dynamic detection range and high detection accuracy of remote sensing instruments are needed for vertical airflow detection.

The lidar has demontrated to be a useful tool for atmospheric research. Today, lidar techniques for remote sensing of atmospheric temperature profiles have reached the maturity necessary for routine observations (Behrendt et al., 2002; Wu et al., 2016). Lidar has been used for the evaluation of the vertical air velocity near and inside the cloud deck (Lottman et al., 2001), and the millimeter-wave radar has also used for the detection of vertical air motions (Kollias et al., 2002). The coherent Doppler lidar estimates the radial component of the velocity from the Doppler frequency or mean frequency of the backscattered laser field based on atmospheric aerosol particles. The performance of the coherent Doppler lidar is determined by the systematic and random errors of the estimates of the mean frequency, which is related to the radial component of the velocity. The detection accuracy of the coherent lidar regarding the radial velocity can reach the order of cm (Frehlich et al. 1994). Lidar instruments can detect vertical air motions at the cloud base (Lottman et al., 2001), but due to the weak penetration of lasers into clouds and fog, the speed of a thick cloud top cannot be measured by lidar instruments. Compared to the lidar, the millimeter-wave radar achieves a stronger ability to detect clouds. The millimeter-wave radar has the advantages of a high sensitivity and strong penetration. This instrument can measure the motion state inside the cloud. The cloud top height, cloud base height, and cloud dynamic parameters (such as the vertical velocity of airflow) can be obtained with the millimeter-wave radar. The small-particle tracing method has been used to obtain the vertical air velocity in clouds with the millimeter-wave radar. The detection resolution of the millimeter-wave radar is on the order of centimeters (Jiafeng et al., 2017), and the detection accuracy is on the order of decimeters (Shupe et al., 2008). Regarding stratiform clouds with low rising speeds, the lidar instrument should be used to detect the vertical air velocity at the cloud base. Regarding convective clouds with higher rising speeds, the millimeter-wave radar can also be used to detect the vertical air velocity at the cloud base.

Lidar (rotational Raman Lidar or high-spectral resolution Lidar) and microwave radiometers have been developed to observe temperature and relative humidity profiles. With the rotational Raman lidar, temperature measurements can be carried out not only in the clear atmosphere but also in aerosol layers and optically thin clouds (Cooney, et al. 2016; Su et al., 2013). The temperature detection accuracy of the rotational Raman lidar exceed 1 K in low-altitude areas. Regarding thick clouds, it is necessary to use a microwave radiometer to obtain the temperature profile in the cloud or at the cloud top. Compared to

175 lidar instruments, the range resolution and detection accuracy of microwave radiometers are low, but their maximum detection distance can reach 10 km and cover the top of most clouds.

Lidar, millimeter-wave radar and microwave radiometers should be used together to realize continuous observation of the vertical air velocity and temperature at the cloud base and cloud top with high temporal and spatial resolutions. The temperature at and below the cloud base can be obtained with a lidar instrument, and the value at the cloud top (if the cloud

180 top height is less than 10 km) can be obtained with a microwave radiometer. The vertical velocity can be measured with the millimeter-wave radar. Fig. 2 shows the technical route of remote sensing observations for atmospheric column condensate evaluation. Temperature data retrieved from a sounding balloon are used to calibrate the measurement results obtained with the Raman lidar and microwave radiometer.
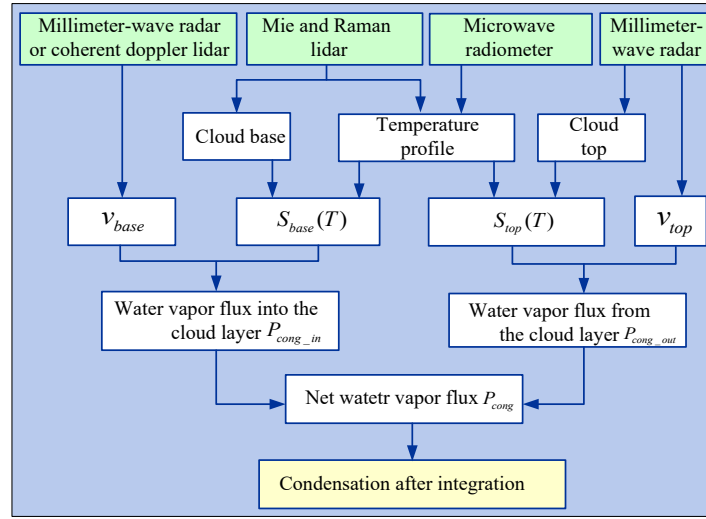
185 **Figure 2: Technical route of remote sensing observations for atmospheric column condensate evaluation**

Although lidar and millimeter-wave radar instruments have the advantages of high spatiotemporal resolution, their detection accuracy for temperature and wind speed is affected by the system signal-to-noise ratio (SNR), which can affect the quantification accuracy of atmospheric column condensate. The determination of atmospheric column condensate depends on the water vapor flux into the cloud. According to the standard error propagation method, the uncertainty in the water

190 vapor flux $\sigma_{p_{wv}}$ depends on the input and output flux errors $\sigma_{p_{wv\_in}}$ and $\sigma_{p_{wv\_out}}$. These errors are determined by the uncertainty in the wind speed σ_v and the saturated water vapor density σ_S and $\sigma_{p_{wv\_in}}$ and $\sigma_{p_{wv\_out}}$ can be written as the following equations on the assumption that σ_S and σ_v do not vary with time and are independent of each other.

$$\sigma_{p_{wv\_in}} = \sqrt{\sigma_{S_{base}}^2 \cdot \overline{v_{base}}(t)^2 + \sigma_{v_{base}}^2 \cdot \overline{S}_{base}^2(T,t)} \tag{9}$$

$$\sigma_{p_{wv\_out}} = \sqrt{\sigma_{S_{top}}^2 \cdot \overline{v_{top}}(t)^2 + \sigma_{v_{top}}^2 \cdot \overline{S}_{top}^2(T,t)} \tag{10}$$

The overline mean the average of parameters in a short measurement period. The uncertainty in the saturated water vapor density depends on the temperature accuracy σ_T. The standard deviation can be obtained according to Equations (11) to (13):

$$\sigma_S = \frac{dS(T)}{dT} \cdot \sigma_T, \tag{11}$$

$$\frac{dS(T)}{dT} = \frac{2.17(T+273.15) \cdot \frac{de(T)}{dT} + 2.17e(T)}{(T+273.15)^2}, \tag{12}$$

$$\frac{de(T)}{dT} = \frac{610.8 \times 17.27(2T+237.3)}{(T+237.3)^2} \cdot \exp\left(\frac{17.27T}{T+237.3}\right), \tag{13}$$

The detection uncertainty of the instantaneous atmospheric column condensate varies with the cloud base temperature. The temperature uncertainty of the lidar at the cloud base ranges from 0.5 to 1 K, and the measurement uncertainty of the wind speed is lower than 0.1 m/s. Choosing spring in northern China as an example and assuming that the ground surface temperature is 15 °C and the height of the cloud base is 3 km, the temperature of the cloud base ranges from approximately -3°C to -4°C. The standard deviation of the lidar for water vapor flux detection is approximately 0.7 $g/m^2 \cdot s$ according to Equations (9) to (13):

5 Instrumentation

The ground-based instruments used in this study are as follows: millimeter-wave radar, which provides reflectivity and Doppler spectrum data; microwave radiometer, which provides temperature profile; lidar, which can provide the temperature, humidity profile, particle polarization characteristics, etc. These detection devices are installed at the Atmospheric Exploration Centre of the China Meteorological Administration. As shown in Fig. 3, the microwave radiometer and millimeter-wave radar are placed next to each other, approximately 50 m away from the lidar. The launch site of the sounding balloon occurs only 10 m from the lidar. Compared to the observation target, the distance between these devices is approximately negligible, so this step provides a reliable research basis for subsequent joint observation and data inversion.
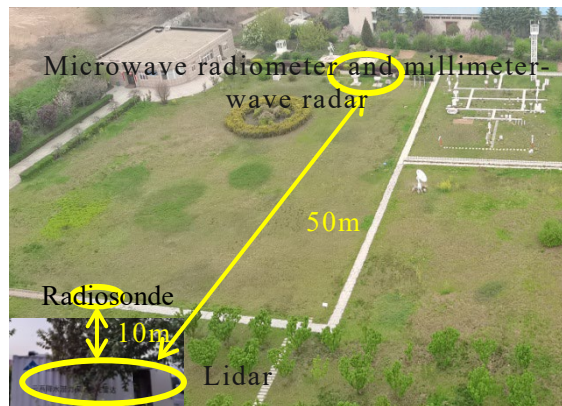
Figure 3: Installation of the equipment at the observation points

6. Remote sensing technology of the atmospheric temperature and vertical airflow velocity

6.1 Rotational Raman lidar for temperature profiles

An ultraviolet rotational-vibrational-Mie Raman lidar system was established at Xi'an University of Technology (34.233°N, 108.911°E) in 2019. The ultraviolet wavelength of 354.7 nm was chosen to enhance the vibrational-rotational Raman signals, as the intensity of molecular scattering is sensitive to the wavelength of the incident light. This lidar system employs a Nd:YAG pulsed laser as the light source. The output energy at a frequency-tripled wavelength of 354.7 nm is ~220 mJ at a 20 Hz repetition rate with the 9 ns FWHM pulse duration. The laser beam divergence reaches approximately 0.3 mrad. The receiver is constructed using a Cassegrain telescope with a diameter of 400 mm and a focal length of 2000 mm. The collected lidar returns are coupled into a multimode fiber optic and guided into a high-efficiency spectroscopic box. All signals were detected by photomultiplier tubes. Two pure rotational Raman signals with different temperature dependences of the central wavelengths of 352.5 and 353.9 nm were selected to retrieve atmospheric temperature profiles. A set of dichroic mirrors and narrow-band interference filters with narrow angles of incidence was utilized to construct a high-efficiency 5-channel polychromator. The lidar system could detect temperatures at heights from 0.5~5 km under clear-sky or thin-cloud conditions. In addition to the temperature, the cloud base height is important. An improved differential zero crossing method (Mao et al., 2010) was used for the retrieval of the cloud base height.

Fig. 4 shows a set of range-squared-corrected signals (RSCSs) (Fig. 4(a)) and temperature profile data retrieved from rotational Raman signals under cloudy weather conditions detected with the lidar. The height of the cloud base was approximately 4.5 km. The figure also shows radiosonde data and the absolute deviation during the same period (Fig. 4(b)). Fig. 4(b) shows the retrieved temperature data at 0.7 km from the cloud base to the inside of the cloud, and there occured a good match between the lidar and radiosonde data. The absolute deviation near the cloud base was less than 1 K. Due to the influence of overlap, the temperature below 1 km exhibited a large deviation. Because this paper focuses on the temperature at the cloud base, the deviation of the base layer was not considered. Fig. 4 (c) shows the temperature statistical error calculated according to the signal-to-noise ratio (SNR) of the lidar. The temperature uncertainty near the cloud base was less than 0.5 K. To further estimate the reliability of the Raman lidar, we used 50 sets of temperature profiles to perform regression analysis between the lidar and radiosonde data. As shown in Fig. 5, the correlation coefficient reached 0.98 below a height of 5 km, and the root mean square error was 1.2 K.
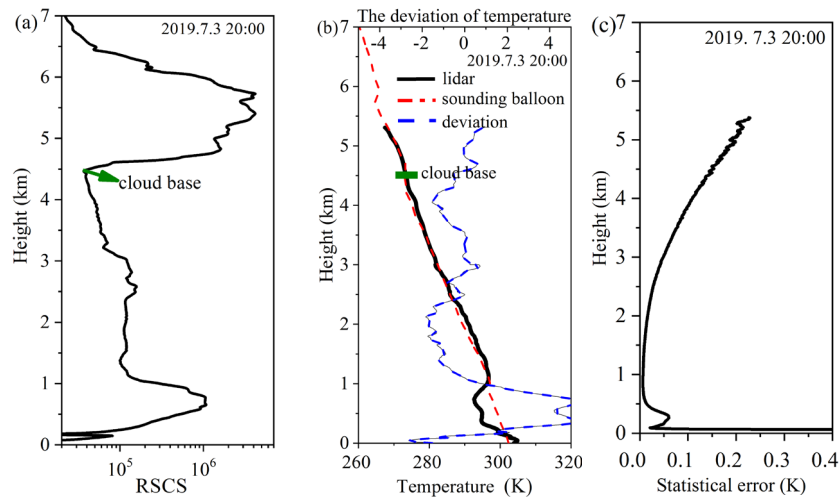
Figure 4: Mie-scattering signal (a), temperature profile (b) and statistical error (c) detected by the rotational Raman lidar
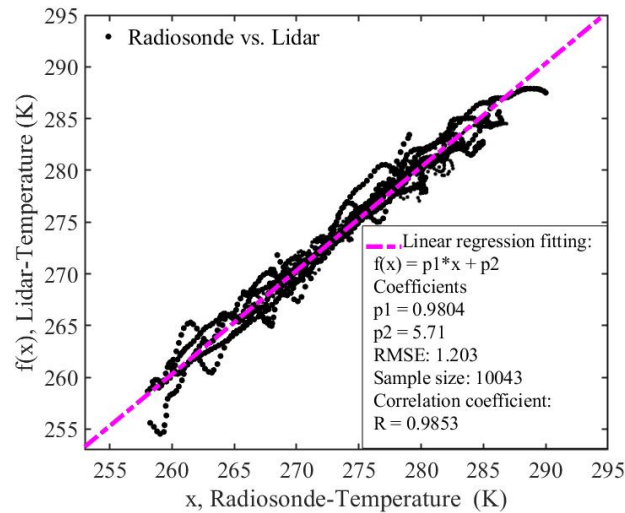
Figure 5: Regression analysis between the Raman lidar and radiosonde data and root-mean-square of the temperature

6.2 Millimeter-wave radar for the vertical airflow velocity

The vertically pointing 35-GHz millimeter-wave radar (Williams et al., 2016) is often used in cloud research. The size of cloud particles is related to their natural falling velocity of cloud particles. The radial velocity measured by the vertically pointing millimeter-wave radar includes the falling velocity of cloud particles in a static atmosphere and atmospheric vertical velocity. Regarding micron-scale cloud particles, the natural falling speed is very low (within 2 cm/s), and the vertical motion speed of air can be 1~2 orders of magnitude larger than that of cloud particles (Kollias et al., 2001; Kollias et al., 2011).

Both vertical air motion and particle falling speed contribute to the Doppler velocities measured by cloud radars (Gossard et al., 1996). Moreover, the spectrum of radar Doppler velocities is influenced by turbulence within the radar volume. Thus, the derivation of vertical air motions from vertically oriented cloud radar measurements is only possible under specific sets of conditions. First, with explicit knowledge of the cloud particle size distribution, a quiet-air spectrum of particle falling speeds can be computed and can then be compared to the measured radar Doppler spectrum to provide an estimate of vertical air motion (O'Connor et al., 2005). Quiet-air Doppler spectra can also be determined by deconvolving the falling speed and turbulent contributions to the measured radar Doppler spectrum. These methods rely on assumptions regarding the shape of the particle size distribution and the particle size-falling speed relationship (Gossard 1994; Gossard et al., 1996) and/or computationally intensive inversion processes (Babb et al. 1999). If only the vertical velocity is desired, a much simpler retrieval method can be applied that only requires prior knowledge on the presence of small particles, such as liquid water cloud droplets, in the radar volume that are assumed to be tracers of clear-air motion(Gossard 1994; Kollias et al., 2001; Shupe et al., 2008). Here, we exploit this last condition to derive vertical air velocities from cloud radar measurements.

Assuming that the vertical motion of the atmosphere is uniform during millimeter-wave radar detection, the Doppler velocity from small to large corresponds to the particle size from small to large. The size distribution of supercooled liquid droplet is relatively narrow, their spectrum can be closely approximated by a Gaussian model. Then the first spectral point on the left side of the power spectrum represents the signal of the smallest particle that can be detected by the radar. As shown in Fig. 6, W_{air} is the vertical velocity of the air.
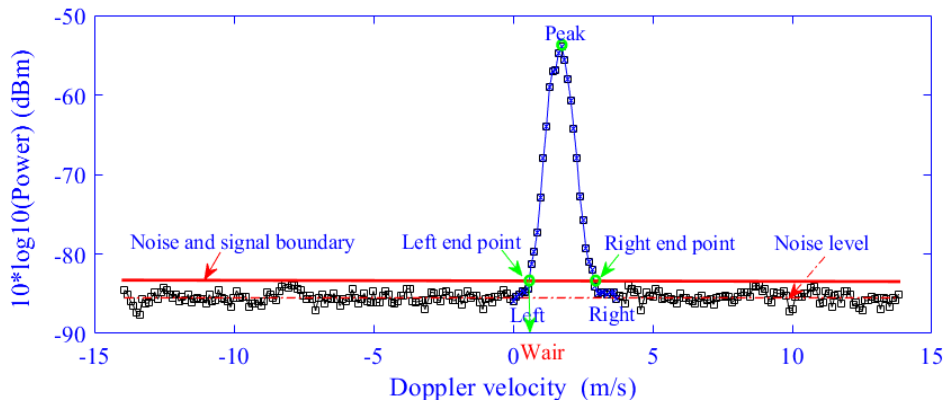
Figure 6: Schematic diagram of power spectrum data processing

Precise wind field measurement under rainy conditions is a challenge due to the presence of interfering signals resulting raindrop reflections (Kollias et al., 2014). Precipitation particles often occur in cloud layers, so it is very important to distinguish the falling velocity of raindrops and the vertical airflow velocity. Under rainy conditions, the received backscattering signal contains two components, the cloud particle signal and the precipitation particle signal. Two peaks of the Doppler power spectrum can be observed if the wind and rainfall velocities differ. The vertical airflow and raindrop falling velocity can be distinguished according to the difference in their power spectra.

7. Case study of the observation of atmospheric column condensate

7.1 Joint detection of clouds with remote sensing instruments

280   Stratiform clouds were observed with the lidar and millimeter-wave radar during the period from June 8, 2021, to June 9, 2021. During this period, a weak rainfall process occurred, and clouds dissipated later. Fig. 7(a) shows the RSCSs at 1064 nm from the lidar, and Fig. 7(b) shows the results of the millimeter-wave radar.
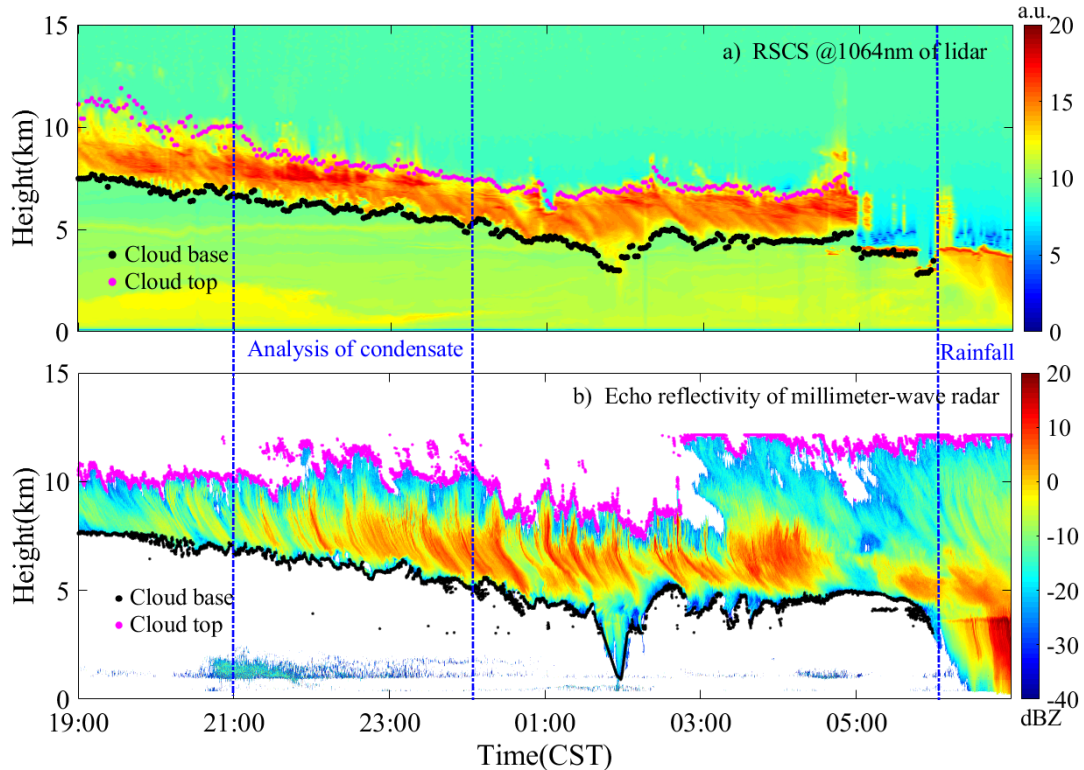
Figure 7: Time-height-indicator (THI) plots of the range-squared-corrected signal (RSCS) observed by the lidar at 1064 nm; (b)
285   **time-height-indicator (THI) plots of the reflectivity observed by millimetre-wave radar.**

According to Fig. 7, the cloud layer was detected simultaneously by the lidar and millimeter-wave radar, and the cloud base height decreased from ~ 8 km to ~ 0.5 km during the observation period. The cloud base height was maintained at approximately 5 km from 02:00 to 05:00 on June 9, 2021, while the cloud thickness increased. There was rain on June 9, 2021. The lidar could not effectively detect rainfall. However, cloud changes during rainfall were effectively observed by
290   millimeter-wave radar. The penetration ability of millimeter-wave radar is greater than that of the lidar. The value distribution equalization (Zhao et al., 2014) method was used to calculate the cloud base height change detected by the lidar (the black mark in Fig. 7 (a)). Based on the millimeter-wave radar detection mechanism (Matthew et al., 2007), the cloud base and cloud top of the millimeter-wave radar were derived (Fig. 7 (b)). The black points represent the cloud base, and the flat red points represent the cloud top. Because the penetration ability of lidar is not as good as that of the millimeter-wave

295   radar, the height of the cloud top is subject to the detection result of the millimeter-wave radar. The cloud base height values detected by the two devices are shown in Fig. 8. The cloud base height and its change trend detected by the two devices exhibit a high degree of coincidence during the observation period (before rainfall). Correlation analysis was carried out. The results are shown in Fig. 8, and the correlation was 0.9256. It is verified again that these two devices provide a certain consistency in the macroscale parameters of clouds in the process of joint observation.

300   (a)   (b)
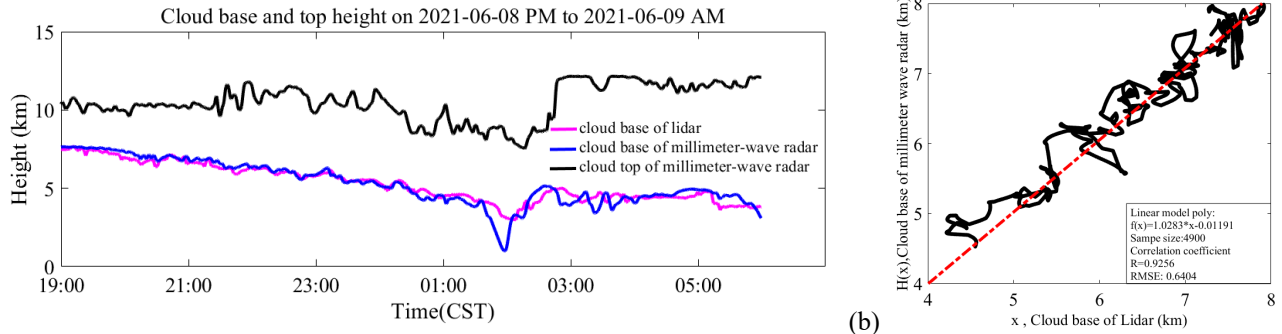
Figure 8: Cloud base heights detected by the lidar and millimeter-wave radar. (a) Time series of the cloud base height, (b) correlation analysis of the cloud base height

During the period of observation, the cloud phase state also changes with the cloud thickness and height. Through discrimination and identification of the cloud phase state in the observation process (Shupe et al., 2008), it was determined

305   that the cloud phase state was a mixed phase state from 21:00 to 23:59 on June 8, 2021, and the state remained relatively stable. The base of the cloud was a liquid water area. During this detection period, the small- particle tracing method could be used to accurately obtain the W_{air}, which could improve the accuracy of condensate determination. During the period of 21:00-23:59 (it is marked with blue dotted line in Fig. 7), the temperature and vertical velocity of the cloud boundary were detected, and the saturated water vapor density of the cloud boundary was calculated according to the temperature. The water

310   vapor flux into the cloud during this period, that is, the maximum possible condensate, was deduced. From figures 7 and 8, the cloud bottom height keeps falling, indicating that water vapor is constantly replenished into the clouds and condensed water was generated. The column condensate after 23:59 is not calculated in this paper, mainly because the vertical velocity calculated by the minimum particle tracing method of millimeter-wave radar is inaccurate, which will introduce large calculation deviation.

315   **7.2 Temperature and vertical wind velocity at the cloud base and top**

The temperature information below the cloud was retrieved according to the rotational Raman signal of lidar. Combined with the cloud base position, a time series of the cloud base temperature was obtained. The temperature at the cloud top cannot be detected by lidar. Microwave radiometer data were chosen as a supplement for temperature determination. The results of the microwave radiometer were validated against sounding balloon data, and the temperature deviation of the microwave

radiometer was less than 2 K. A time series of the cloud top temperature was also derived. The temperature results at the cloud base and top (2021-06-08 21:00-23:59) are shown in Fig. 9.
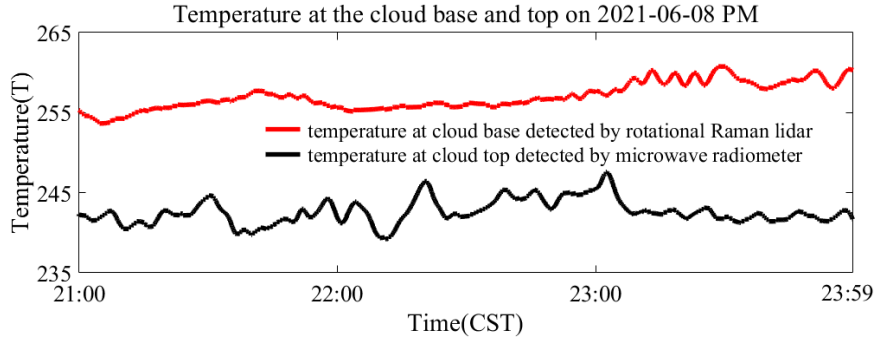
Figure 9: Time series of the temperature at the cloud base and top

The power spectrum data of the millimeter-wave radar from 21:00 to 23:59 on June 8, 2021, were ananlyzed, and the air vertical motion velocity at the cloud base and cloud top (positive upward and negative downward) was obtained via the small-particle tracing method described above (Subsection 6.2). The results are shown in Fig. 10. The calculated atmospheric vertical velocity value is relatively consistent with Matthew (Matthew et al., 2007). Fig. 10 shows that there mainly occured updraft at the cloud base, and the updraft and downdraft processes at the cloud top were staggered, but mainly the downdraft process, which is also in line with the phenomenon of cloud top height decline.
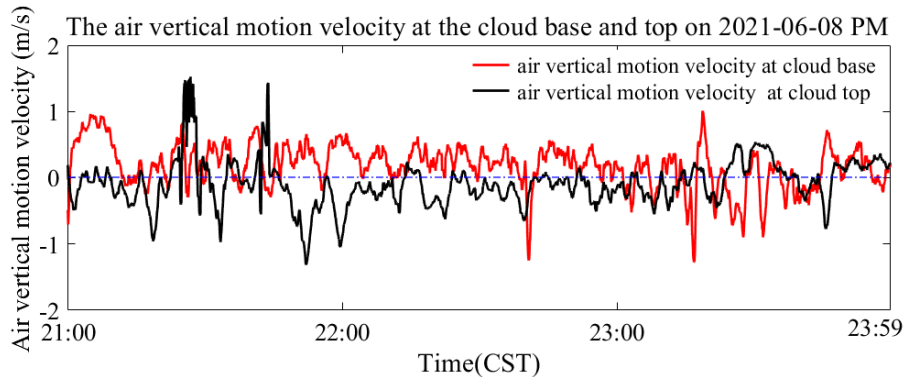
Figure 10: Time series of the air vertical motion velocity at the cloud base and cloud top

7.3 Results of atmospheric column condensate

The water vapor flux was calculated according to Equations (2)-(8). As shown in Fig. 10, the cloud top temperature was approximately 12°C ~15°C lower than the cloud base temperature; therefore, it could be considered that the water vapor remaining in the cloud could condense to a large extent. The rising air at the cloud top brings water vapor out, reducing condensate content in the cloud. Fig. 11 shows the water vapor flux through the cloud base and cloud top. In this observation, both water vapor entering from the cloud base and water vapor leaving from the cloud top in this observed case. The water vapor flux entering the cloud base minus the water vapor flux leaving the cloud top is the value remaining in the cloud layer, which could be considered the maximum possible condensate flux. If the water vapor flux is positive, the cloud is constantly

340 generating and developing, and if the flux is negative, the cloud is dissipating. Fig. 12 shows the instantaneous water vapor flux remaining in the cloud layers.
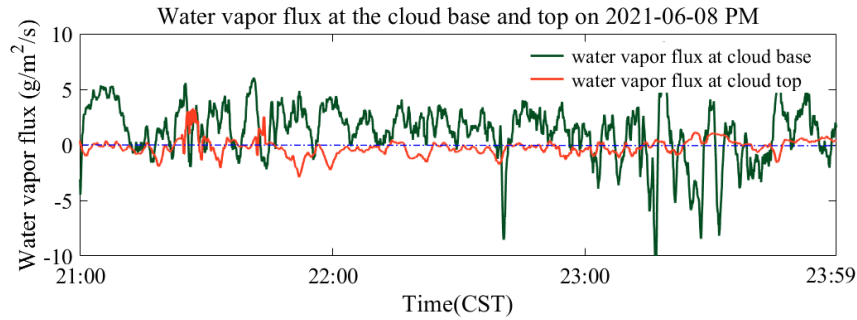
Figure 11: Time series of the water vapor flux at the cloud base and top
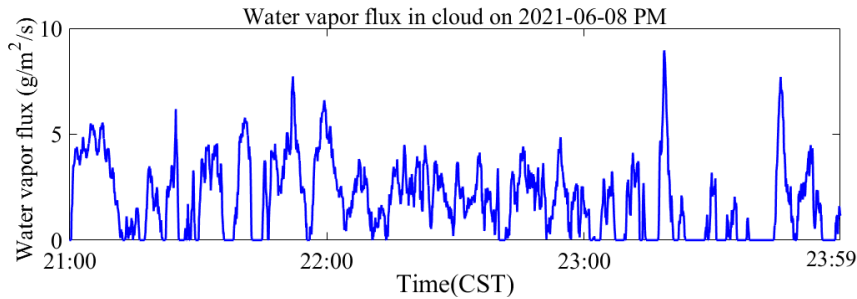
345 **Figure 12: Instantaneous water vapor flux remaining in the cloud layer**

The atmospheric column condensate could be obtained by integrating the instantaneous water vapor flux. Fig. 13 shows the hourly condensate during the observation period. As shown in Fig. 11, updraft at the cloud top was very limited, so it could be considered that the water vapor entering the cloud basically remained in the cloud. According to Eq. (5), the condensate over the period from 21:00 to 23:59 was integrated, and it could be found that the total amount of the maximum possible

350 condensate in the atmosphere during this period was approximately 88.2 g/m^2 (2.94 mm/m^2). The water condensed during this period provided resources for the incoming rainfall at 06:00 a.m. on June 9, 2021. Therefore, the detection and derived results are in good agreement with the changes in weather and clouds on this day.
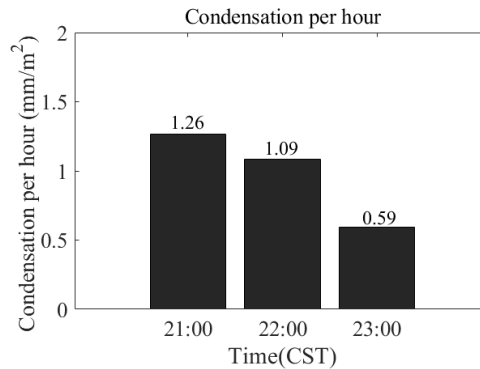
Figure 13: Hourly condensate during the observation period

8. Results and discussion

It is very difficult to directly measure atmospheric column condensate. According to the characteristics of different remote sensing equipment, the condensate content can be deduced by measuring meteorological parameters near and inside the cloud deck. This paper presents a remote sensing method for atmospheric column condensate detection by using lidar, millimeter-wave radar and microwave radiometer instruments. A detailed detection scheme and data calculation method are given. A precipitation process was observed, and atmospheric column condensate was obtained by active and passive instruments. In this method, it is considered that the water vapor remaining in the cloud can condense, which is an ideal assumption. In fact, a part of the water vapor entering the cloud evaporates or exits the cloud boundary, which can lead to a reduction in the condensate. These effects are not considered in this paper. We provide the maximum possible atmospheric column condensate. Therefore, the derived condensate should be larger than the actual value. Nevertheless, the method proposed in this paper remains valuable. The method proposed in this paper only uses observation data at one point to represent the results throughout the whole region, which is reasonable for horizontally uniform stratiform clouds. Regarding clouds with strong convection, it is more effective to use multipoint network observation data.

Stratiform clouds often appear in northern China and are the main targets of artificial weather modification. The vertical airflow velocity under stratiform clouds is low and should be obtained with high-precision detection equipment. The lidar is an effective instrument to obtain high-precision wind speed and temperature data below clouds. Precipitation involves a complex weather system that can be divided into two categories: convective precipitation and systematic precipitation. Convective precipitation generally covers a small range. The horizontal scale of convective clouds is on the order of 100 km, and the water vapor supply is mainly provided by the rise of air near the ground. Updraft before precipitation can be measured with the millimeter-wave radar or lidar to obtain the potential precipitation, namely, the total amount of cloud water in a certain area and a certain period of time. After the beginning of precipitation, if the precipitation is very low, a lidar instrument can also detect the temperature and updraft in the precipitation area, but when there is heavy precipitation, lidar cannot obtain effective data. Systematic precipitation is complex, and a multilayer cloud structure can emerge. Lidar instruments usually cannot penetrate multilayer clouds, and these devices are only suitable for the detection of the base of single-layer clouds. In terms of multilayer clouds, it is necessary to use the millimeter-wave radar to detect the vertical air velocity in multilayer clouds and a microwave radiometer to detect the temperature in clouds.

The assessment of CWRs in an area requires long-term statistical results, which necessitate long-term continuous remote sensing observations. This paper provides a detection method for atmospheric column condensates and a scientific observation case. More cloud observation results will be carried out in the future for CWRs assessment.

Data availability

Data and code related to this article are available upon request to the corresponding author.

Author contributions

The conceptualization was performed by HD and DH. The methodology and investigation were completed by HD, YY, QY, WX,JW and SL. HD drafted the original manuscript, which was reviewed and edited by YY, HD. YW contributed to significantly improve the manuscript. Supervision was the responsibility of DH and LZ, and project administration by DH.

Competing interests

The authors declare that they have no conflict of interest.

Acknowledgements

We are very grateful to Jietai Mao (Peking University) for providing the useful suggestions and interpretation and definition of atmospheres cloud-water resources for this manuscript, and we are thankful to the Xi'an Meteorological Administration of China for supporting the data collection and archiving.

Financial support

This research has been supported by National Natural Science Foundation of China (NSFC): 41627807. National Natural Science Foundation of China (NSFC): 42130612.

References

Behrendt, A. & Nakamura, T.: Calculation of the calibration constant of polarization lidar and its dependency on atmospheric temperature. Opt Express., 10(16), 805-17, doi:10.1364/OE.10.000805,2002.

Cooney, & John.: Measurement of atmospheric temperature profiles by raman backscatter. J Appl Meteorol Clim., 11(1), 108-112, doi:10.1175/1520-0450 (1972)011<0108:moatpb>2.0.co;2,1972.

Edward P. Luke,Pavlos Kollias.: Separating Cloud and Drizzle Radar Moments during Precipitation Onset Using Doppler Spectra. J Atmos Ocean Tech., 30,1656-1671, doi:10.1175/JTECH-D-11-00195.1, 2012.

Frehlich, R., Hannon, S. M., & Henderson, S. W.: Performance of a 2-m coherent doppler lidar for wind measurements. J.atomos.oceanic Technol.,11(11), 1517-1528. doi:10.1175/1520-0426(1994)0112.0.CO;2,1994.

Gossard, E. E., Snider, J. B., Clothiaux, E. E., Martner, B., & Frisch, A. S.: The potential of 8-mm radars for remotely sensing cloud drop size distributions. J Atmos Ocean Tech.,14(1),76-87,doi:10.1175/1520-0426(1997)014<0076:TPOMRF>2.0.CO;2,1996.

415

Gossard, E. E.: Measurement of cloud droplet size spectra by doppler radar. J Atmos Ocean Tech., 11(3), 712-726, doi:10.1175/1520-0426(1994)0112.0.CO;2,1994.

Gu, X., & Bing, Z.: Vapor sink and latent heat of condensation in the atmosphere and the parameterization of cumulus

420 convection. Acta Meteorol Sin., 64(6), 790-795,doi:10.1016/S1872-2032(06)60022-X,2006.

Hengchi, L., Dezhen, J., Chong, W., & Zhilai, S.: An airborne microwave radiometer and measurements of cloud liquid water. Chinese Sci Bull., 48(0z2), 82-87, doi:10.1360/03wd0462,2003.

Jalihal, C., Srinivasan, J., & Chakraborty, A.: Modulation of indian monsoon by water vapor and cloud feedback over the

425 past 22,000 years. Nat. Commun., 10:5701, doi:10.1038/s41467-019-13754-6,2019.

Jiafeng, Z., Liping, L., Keyun, Z., Jingya, W., & Binyun, W.: A method for retrieving vertical air velocities in convective clouds over the tibetan plateau from tipex-iii cloud radar doppler spectra. Remote Sens.,9, 964,2-17, doi:10.3390/rs9090964,2017.

430

Kollias, P., Albrecht, B. A., & F Marks.: Why mie? accurate observations of vertical air velocities and raindrops using a cloud radar. Bull.amer.meteor.soc., 83(10), 1471-1483, doi:10.1175/BAMS-83-10-1471,2002.

Kollias, P., Albrecht, B. A., Lhermitte, R., & Savtchenko, A.: Radar observations of updrafts, downdrafts, and turbulence in

435 fair-weather cumuli. J Atmos Sci.,58(13),1750-1766, doi:10.1175/1520-0469(2001)0582.0.CO;2,2001.

Kollias, P., Jasmine Rémillard, Luke, E., & Szyrmer, W.: Cloud radar doppler spectra in drizzling stratiform clouds: 1. forward modeling and remote sensing applications. J Geophys Res-Atmos., 116 ,D13201,doi:10.1029/2010JD015237,2011.

440 Liu, F., & Yi, F.: Spectrally resolved raman lidar measurements of gaseous and liquid water in the atmosphere. Appl Opt., 52(28),6884-6895, doi:10.1364/AO.52.006884,2013.

Liu, W. Q., Chen, Z. Y., Liu, J. G., & Xie, P. H.: Stereoscopic monitoring technology and applications for the atmospheric environment in China. Chinese Sci Bull., 61(30), 3196-3207, doi:10.1360/N972016-00394,2016.

445

Lottman, B. T., & Frehlich, R. G.: Evaluation of vertical winds near and inside a cloud deck using coherent doppler lidar. J Atmos Ocean Tech., 18(8), 1377-1386, doi:10.1175/1520-0426 (2001)0182.0.CO;2,2001.

Mao F, Gong, W., Li, J., & Zhang, J.: Cloud detection and parameter retrieval based on improved differential zero-crossing method for mie lidar. Acta Optica Sinica.,30(11),3097-3102, doi:10.3788/AOS20103011.3097,2010.

MATTHEW D. SHUPE, PAVLOS KOLLIAS, P. OLA G. PERSSON, GREG M. MCFARQUHAR.: Vertical Motions in Arctic Mixed-Phase Stratiform Clouds. J Atmos Sci., 65,1304-1322, doi:10.1175/2007JAS2479.1,2007.

O'Connor, E. J., Hogan, R. J., & Illingworth, A. J.: Retrieving stratocumulus drizzle parameters using doppler radar and lidar. J Appl Meteorol Clim., 44,14-27, doi:10.1175/JAM-2181.1,2005.
Pavlos, Kollias, Wanda, Szyrmer, Jasmine, & Rémillard.: Cloud radar doppler spectra in drizzling stratiform clouds: 2. observations and microphysical modeling of drizzle evolution. J Geophys Res., 116(D13) , doi:10.1029/2010jd015238,2011.

Shupe, M. D., Kollias, P., Poellot, M., & Eloranta, E.: On deriving vertical air motions from cloud radar doppler spectra. J Atmos Ocean Tech., 25(4), 547-557, doi:10.1175/2007JTECHA1007.1,2008.

Si, A., Ts, A., Ho, B., Ks, B., Sk, B., & Mf, C., et al.: Large-and-sparse-particle clouds (lsc): clouds that are subvisible for space-borne lidar and observable for space-borne cloud radar. Polar Sci., 21, 117-123, doi:10.1016/j.polar.2019.05.003,2019.

Su T., & Feng G.L.: The characteristics of the summer atmospheric water cycle over China and comparison of ERA-Interim and MERRA reanalysis.Acta Phys Sin., 63(24),493-505,doi:10.7498/aps.63.249201,2014.

Su, J., Mccormick, M. P., Wu, Y., Lee, R. B., Lei, L., & Liu, Z.: Cloud temperature measurement using rotational raman lidar. J Quant Spectrosc Ra., 125, 45-50, doi:10.1016/j.jqsrt.2013.04.007,2013.

Williams, C. R., Beauchamp, R. M., & Chandrasekar, V.: Vertical air motions and raindrop size distributions estimated using mean doppler velocity difference from 3- and 35-ghz vertically pointing radars. IEEE T Geosci Remote.,54(10),1-13,doi:10.1109/TGRS.2016.2580526,2016.

Wu, D., Wang, Z., Wechsler, P., Mahon, N., & Heesen, B.: Airborne compact rotational raman lidar for temperature measurement. Opt Express., 24(18), A1210- A1223, doi:10.1364/OE.24.0A1210,2016.

Yao J.Q., Chen Y.N., Zhao Y., Guan X.F., Mao W.Y., & Yang L.M.: Climatic and associated atmospheric water cycle changes over the Xinjiang, China. J Hydrol.,585, 124823, doi:10.1016/j.jhydrol.2020.124823,2020.

Yoshiaki, S., MD Yamanaka, Hiroyuki, H., Akira, W., Hiroshi, U., & Yasuyuki, M.: Hierarchical structures of vertical velocity variations and precipitating clouds near the baiu frontal cyclone center observed by the mu and meteorological radars. J Meteorol Soc Jpn.,75(2), 569-596, doi:10.2151/jmsj1965.75.2_569,2009.

Zhao, C., Wang, Y., Wang, Q., Li, Z., Wang, Z., & Liu, D.: A new cloud and aerosol layer detection method based on micropulse lidar measurements.J. Geophys. Res. Atmos., 119,6788–6802, doi:10.1002/2014JD021760,2014.

Zhou Y. Q., Cai M., OU J.I., Cai Z. X., & Shi A.L.: Correlation between cloud characteristic parameters and precipitation. J Atmos Sci., 34(6):641-652, doi:10.3969/j.issn.1674-7097.2011.06.002,2011.

Zhou, L., Liu, Q., Liu, D., Xie, L., Qi, L., & Liu, X.: Validation of modis liquid water path for oceanic nonraining warm clouds: implications on the vertical profile of cloud water content. J Geophys Res-Atmos., 121(9), 4855-4876, doi:10.1002/2015JD024499,2016.

Zhou, Y., Cai, M., Tan, C., Mao, J., & Zhijin, H. U.: Quantifying the cloud water resource: basic concepts and characteristics. J Meteorol Res-Prc.,34(6), 1242-1255, doi:10.1007/s13351-020-9125-7,2020.